Available online at www.sciencedirect.com
ScienceDirect
Journal of the European Ceramic Society 27 (2007) 2203–2208
www.elsevier.com/locate/jeurceramsoc

Phase instability in ZrO_2–TiB_2 composites

Corneliu Sarbu [a,*], Jef Vleugels [b], Omer Van der Biest [b]

[a] National Institute for Physics of Materials, 105-B Atomistilor Street, P.O. Box MG-7, RO-077125 Magurele-Bucharest, Romania
[b] Department of Metallurgy and Materials Engineering, Katholieke Universiteit Leuven, Kasteelpark Arenberg 44, B-3001 Heverlee, Belgium

Received 12 April 2006; received in revised form 14 July 2006; accepted 21 July 2006
Available online 18 September 2006

Abstract

2.5 mol% Y_2O_3-stabilised ZrO_2 composites with 30 vol.% TiB_2 particles, hot pressed in vacuum at 1450 °C, were investigated by means of quantitative electron energy loss spectroscopy (EELS) with a nanobeam analytical field emission gun transmission electron microscope (FEG-TEM). The experimental results revealed that B is diffusing out of the titanium boride grains, forming textured polycrystalline BN agglomerates leaving behind non-stoichiometric TiB_{2-x} single crystal grains. The formation of BN was calculated to be thermodynamically favourable under the actual hot pressing conditions. Boron was also detected in the amorphous intergranular phase, together with Y, Si, O, Al, but not in the ZrO_2 grains. Ti was only detected in the amorphous material in-between the TiB_{2-x} grains and the micro-textured BN grains, but not in the zirconia grains nor in the intergranular amorphous phase in between. There are indications that Ti forms facetted carbide precipitates inside the TiB_{2-x} grains. Zr was not detected in the titanium boride grains, nor in the intergranular amorphous phase in-between the zirconia grains.

Keywords: Hot pressing; Microstructure-final; Electron microscopy; Y-TZP; Borides

1. Introduction

Zirconia is a promising matrix for ceramic composites, but the modest hardness of these composites is limiting their applicability for wear purposes. It has been proposed to overcome this deficiency by the addition of a hard secondary phase.[1] TiB_2 was claimed to be one of the few borides having the required hardness and is expected to be chemically compatible with ZrO_2 at high temperatures.[2] The TiB_2–ZrO_2 system has been investigated during the last decades, but mainly in the range of TiB_2-rich compositions. The available information on Y-TZP-rich composites with less than 50 vol.% of TiB_2 is very limited. The only publication concerns a ZrO_2–TiB_2 (75/25) composite containing more than 80 wt.% or 75 vol.% ZrO_2 and prepared at 1500 °C from zirconia nanopowders stabilised with 1.94 mol% Y_2O_3.[4]

A high strength of more than 800 MPa and toughness of 7–9 MPa $m^{1/2}$ have been reported for composites (TiB_2–30 wt.% ZrO_2) made of pure ZrO_2 and TiB_2, sintered at 1800–1900 °C.[3,4] In order to explain these experimental values, observed in the TiB_2–ZrO_2 system prepared with unstabilised zirconia, the authors claimed that, besides a grain size refinement, a partial stabilisation of the tetragonal ZrO_2 phase as a result of Ti diffusion into ZrO_2 and formation of a (Ti,Zr)B_2 solid solution takes place.[3]

A significant fraction of t-ZrO_2 was observed in TiB_2–30% ZrO_2 composites prepared from stabiliser-free m-ZrO_2 starting powder and sintered at 2073–2173 °C.[5] The observed partial stabilisation of ZrO_2 in these hot pressed 70 vol.% TiB_2 ceramics with unstabilised ZrO_2 is not well understood and may be attributed to a significant amount of Ti in solid solution in the ZrO_2 grains according to the formerly proposed model.[4] On the other hand, it was also suggested that the true Ti concentration in the ZrO_2 grains was overestimated by the energy dispersive X-ray spectroscopy (EDS) analysis method.[5] This was attributed to the effect of X-ray fluorescence generated by the sample in the microscope. EELS data obtained from the same samples revealed that in all cases the Ti concentration in the zirconia grains was below the detection limit.[5]

It is impossible to conclude from the reported experimental results[3–5] whether Ti would always be present in ZrO_2 grains and whether a small concentration of Zr would always be present in the TiB_2 grains, as claimed. Similar doubtful results emerged during an initial microcomposition investigation of our composite samples ZrO_2/TiB_2 (70/30) reported in the present work,

* Corresponding author. Tel.: +40 21 493 01 95; fax: +40 21 493 02 67.
E-mail address: crnl_srbu@yahoo.com (C. Sarbu).

0955-2219/$ – see front matter © 2006 Elsevier Ltd. All rights reserved.
doi:10.1016/j.jeurceramsoc.2006.07.014

done by means of EDS. The EDS X-ray spectra acquired by us in the TEM with the in-hole directed electron beam always showed the presence of a Ti peak of a closely comparable intensity to that acquired with the electron beam directed on the material area of the sample's central hole rim. It is our opinion that the diffusion of Ti out of TiB_2 grains and into ZrO_2 grains is not unequivocally demonstrated in the literature on the ground of the EDS microanalysis data. Therefore, EELS was exclusively used in the present research in order to avoid the disturbing effect of X-ray fluorescence.

Our interest in the microstructure investigation of ZrO_2/TiB_2 (70/30) composites was stimulated by the lack of a suitable explanation of the experimental results showing that the addition of 30 vol.% TiB_2 to an Y-TZP zirconia matrix did not substantially improve the overall hardness of the composite beyond that of the zirconia matrix.[6]

2. Experimental procedure

The ZrO_2–TiB_2 (70/30) studied here is one in a series of Y-TZP based composites with TiB_2, prepared by a new procedure designed for tailoring an excellent transformation toughness of the ZrO_2 matrix.[6] The ZrO_2 matrix of the final ceramic composite was prepared by mixing pure monoclinic zirconia (m-ZrO_2) (Tosoh grade TZ-0) and 3 mol% Y_2O_3 co-precipitated ZrO_2 powder (Tosoh grade TZ-3Y) in the appropriate ratio to reach an overall dopant content level of 2.5 mol% yttria. Commercial TiB_2 powder (H.C. Starck grade E, with an average particle size of 1.5–2.0 μm) was used as secondary phase. The impurity content of the TiB_2 powder is, according to the supplier, C (≤0.25 wt.%), O (≤2.0 wt.%) and N (≤0.25 wt.%) in addition to Fe (≤0.25 wt.%) and other metallic impurities (≤0.2 wt.%).

Fifty to 100 g of mixed powder, with a ZrO_2/TiB_2 volume ratio of 70/30, was mixed on a multidirectional mixer (type Turbula) for 24 h in 1 L of *n*-propanol in a polyethylene bottle. To break the agglomerates in the starting powders, 200 g alumina milling cylinders were added to the container. At the end of the mixing process, the propanol was removed by means of a rotating evaporator.

The dry powder mixture was inserted into a boron nitride coated graphite die having a diameter of 30 mm. After cold pressing at 30 MPa, the samples were hot pressed (W 100/150-2200-50 LAX, FCT, Rauenstein, Germany) in a vacuum of about 0.1 Pa for 1 h under a mechanical load of 28 MPa. The ceramic samples were hot pressed at 1450 °C, with a heating rate of 50 °C/min and a cooling rate of 10 °C/min. The final thickness of the hot pressed samples was about 5 mm.

The samples for TEM investigation were prepared by standard procedures, i.e. laser cutting of 3 mm diameter disks, grinding, dimpling and final ion milling at 5 kV under an incident angle of 12° till perforation. A carbon thin film coating was essential to avoid electrical charging of the sample in the microscope.

In the present investigation we relied exclusively on EELS spectroscopy quantification. An analytical transmission electron microscope (CM-200 FEG, FEI, Eindhoven, The Netherlands) equipped with a Gatan Image Filter (model 678) was used. In most measurements, the fully focussed 1 nm beam (with low convergence angle) was used, whereas occasionally a fully focussed beam of larger diameter (2.2 nm) or a slightly defocused beam to illuminate a circular area of about 100 nm in diameter was applied. The acquisition of EELS spectra was performed in two steps, working in the TEM diffraction mode. In the first step, the low loss part of the spectrum including the zero loss peak was acquired whereas the edges of the elements of interest were acquired in a second step. This experimental procedure was imposed by the dispersion of 0.2 eV/pixel, which emerged as the most reliable in our quantitative analysis. The local contamination was continuously monitored during spectra acquisition by measuring the local thickness variation. The spectra were processed with the standard EL/P v.3.0.2 software supplied by Gatan. The convergence angles to be considered in the calculation were supplied by the microscope manufacturer. A liquid air cooled trap surrounding the sample was used to minimise the local contamination.

3. Results and discussion

3.1. The titanium boride grains

A backscattered electron contrast scanning electron micrograph of the ZrO_2/TiB_2 (70/30) composite is presented in Fig. 1. Three phases can be differentiated, i.e. ZrO_2 (white), TiB_2 (grey) and Al_2O_3 (black). The alumina originates from the milling balls used to break the powder agglomerates during powder mixing.

Fig. 2 shows a representative TEM micrograph of the composite, containing a typically larger sized titanium boride grain surrounded by smaller size zirconia grains. In-between, a ring made of a different material, surrounding the titanium boride grain, is indicated by arrows. The textured microcrystalline structure of this surrounding material is discussed in detail in Section 3.2, where it is shown that it contains B and N atoms in a quantitative ratio close to 1.

The ion milling resulted in a series of titanium boride grains of small angle wedge shape (identified in dark-field contrast by the much largely spaced Fresnel fringes than those observed on the neighbouring zirconia grains), situated on the rim of the main

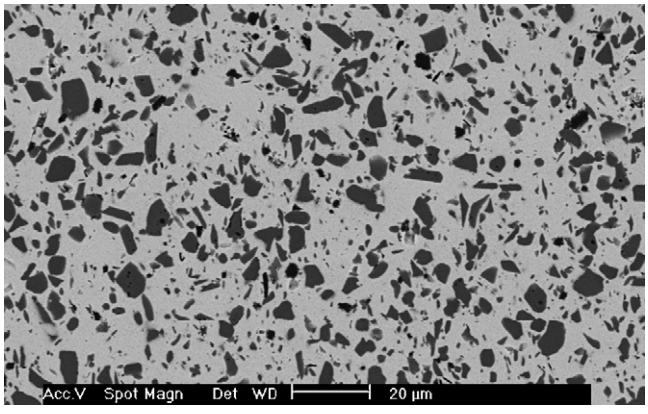

Fig. 1. Backscattered scanning electron micrograph of the ZrO_2/TiB_2 (70/30) composite. ZrO_2 (white), TiB_2 (grey), Al_2O_3 (black).

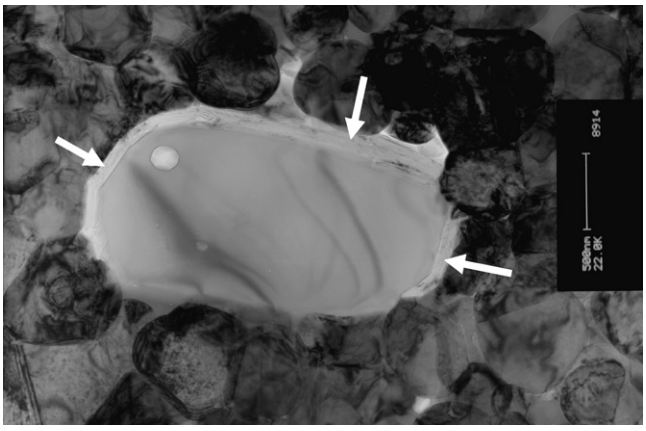

Fig. 2. Bright field image (bar = 500 nm) of a TiB_2 grain in the ZrO_2–TiB_2 composite, surrounded by a ring of a different material, indicated by arrows, whose detailed microtextured structure is shown in Fig. 4.

hole. The small thickness variation in these areas allowed the acquisition of low distorted EELS spectra, which were appropriate for quantification. All titanium boride grains subject to analysis were single crystals, showing electron diffraction spot patterns without any fine structure that could indicate the presence of extended lattice defects.

The EELS analysis data concerning the titanium boride grains of the sintered material are given in Table 1. The electron beam diameter used for illumination of various sample areas is indicated in column (2) for each measurement. The local thickness variation under the beam action, due to contamination growth during spectra acquisition, is indicated in column (3), showing acceptable values. The quality of background subtraction was generally good as indicated by the acceptable values of χ^2 of no more than 50, in spite of the wedge shape of the analysed areas. The composition values resulting from 17 measurements performed at random on five different titanium boride grains, given in column (8) of Table 1, are showing an obvious shift towards higher values of the Ti/B ratio, clearly differing from the value of 0.5 which should be expected for the TiB_2 composition. The mean value calculated from the experimental data is Ti/B = 0.72, revealing a depletion of boron in the titanium boride grains and indicating a significant diffusion of boron out of grains. In our view, a TiB_{2-x} composition formula would be appropriate for describing the detected composition of the titanium boride grains in the compact material.

Large inclusions having geometrically facetted shapes were observed in most of the investigated titanium boride grains, as illustrated in Fig. 3 (similar inclusions, observed at a lower magnification, are visible also in Fig. 2), suggesting a crystal habit. These inclusions were generally too thick to allow accurate quantitative EELS analysis. A rough estimation of the Ti and C content could be done by analysing the rim area of the hole, marked A and indicated by the arrow in Fig. 3. The measured values for Ti and C in the area *A* of the inclusion are 977 ± 98 at/nm^2 and 9460 ± 947 at/nm^2, respectively. No boron was detected. For comparison, the amount of C due to the carbon thin film, as measured on a neighbouring thin grain, was 106 ± 12 at/nm^2. The comparison of the C amounts measured on the two places shows that, besides Ti, the inclusions contain a

Table 1
Quantitative data obtained by EELS, showing the amounts of boron and titanium measured on five grains of titanium boride

Object	Illuminated area[a]	Thickness variation[b] [Fraction of inelastic scattering mean free path]	Measured amount of boron		Measured amount of titanium		Calculated Ti/B ratio	
			No. of B scattering centres (at/nm^2)	Error of no. of B	No. of Ti scattering centres (at/nm^2)	Error of no. of Ti	Calculated Ti/B	Error of calculated Ti/B
(1)	(2)	(3)	(4)	(5)	(6)	(7)	(8)	(9)
Grain 1	C100	ini = 0.5456, fin = 0.6008	6332.36	633.23	4146.85	414.68	0.65	0.09
	C100		6132.00	613.2	4015.64	401.56	0.65	0.09
	FFB1	ini = 0.1714, fin = 0.1792	1865.0	207.09	1298.51	144.56	0.69	0.10
	FFB1		1867.18	207.34	1300.03	144.73	0.69	0.10
	FFB1		1763.84	196.8	1453.0	161.48	0.82	0.12
	FFB1		1765.9	197.03	1454.7	161.67	0.82	0.12
Grain 2	FFB1	ini = 0.2037, fin = 0.3003	1589.11	158.91	1036.69	104.02	0.65	0.09
	FFB1		1525.41	152.54	995.13	99.85	0.65	0.09
	FFB1		1549.65	155.32	1178.38	117.83	0.76	0.10
	FFB1		1487.53	149.09	1131.14	113.11	0.76	0.10
Grain 3	FFB1	ini = 0.5459, fin = 0.5775	4600.63	460.06	3507.76	350.77	0.76	0.10
	FFB1		4536.01	453.6	3458.49	345.84	0.76	0.10
	FFB1		5041.31	504.13	3507.76	350.77	0.69	0.09
	FFB1		4970.5	497.05	3458.49	345.84	0.69	0.09
Grain 4	FFB2.2	ini = 0.3438, fin = 0.3018	5431.66	543.16	3921.53	392.15	0.72	0.10
	FFB2.2		6504.36	650.43	4696.00	468.91	0.72	0.10
Grain 5	FFB2.2	ini = 0.1320, fin = 0.4468	1846.69	184.66	1296.45	129.64	0.70	0.09

[a] C100 means slightly defocussed beam, illuminating a circular area of approximately 100 nm diameter; FFB1 means fully focussed beam of nominal 1 nm beam diameter; FFB2.2 means fully focussed beam of nominal 2.2 nm beam diameter.

[b] ini means initial thickness, measured by using the first acquired spectrum in the series of spectra for quantification; fin means that we have acquired a last spectrum in the series, for the final thickness evaluation.

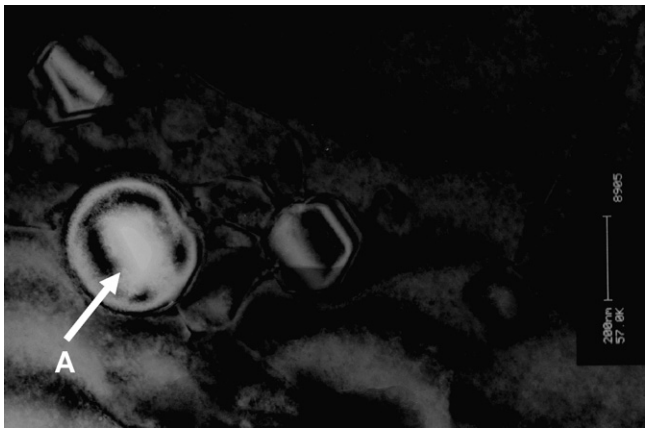

Fig. 3. Inclusions observed in the titanium boride grains, showing a crystal facetted habit. Quantitative EELS analysis of Ti and C was performed on the rim indicated by the arrow. Bar = 200 nm.

large amount of C. No Zr edge was observed in any of the EELS spectra acquired from the TiB_2 grains.

3.2. The new phase containing B and N

Besides the micro-textured agglomerates of crystals surrounding the titanium boride grains, as shown in Fig. 2, other micro-textured agglomerates with a shape as shown in Fig. 4 (marked BN-1 and BN-2) were observed. They are always closely related to the large titanium boride grains. The selected area diffraction pattern, shown as an insert in Fig. 5, is typical for both kinds of observed micro-textured agglomerates of crystals (that of ring shape as shown in Fig. 2 and that of normal grain shape as shown in Fig. 4) and reveals, together with the dark-field contrast image shown in Fig. 5, their micro-textured structure.

The composition measured in three agglomerated grains, having a shape similar to that of the BN grains shown in Fig. 4, on areas similar to that marked by *A* in Fig. 6, are summarised in Table 2. The measured average B/N ratio, calculated from the experimental data in Table 2 is 0.886, being close to 1, as would

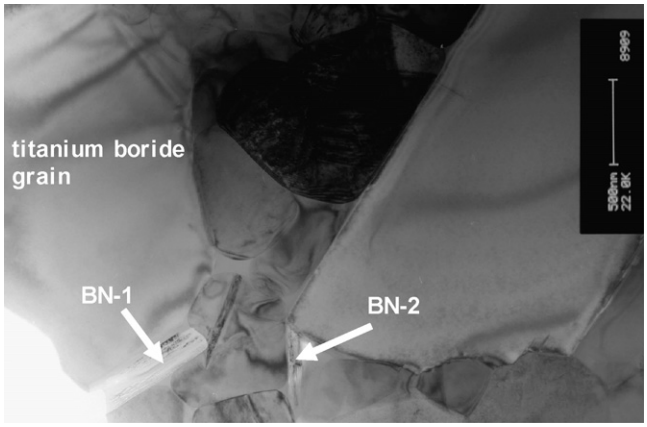

Fig. 4. Bright field image showing the volume extension of two textured microcrystalline agglomerates (marked by arrows) in between large single crystal grains. Bar = 500 nm.

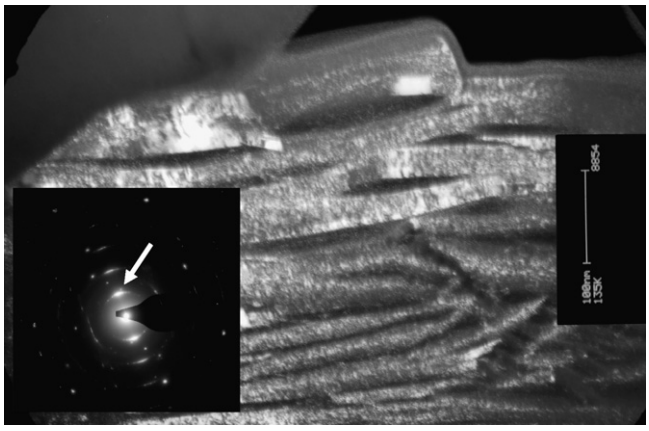

Fig. 5. Dark field image of a textured agglomeration of microcrystallites, taken with the reflection indicated by the arrow in the inserted SAED pattern. Bar = 100 nm. The pattern of spread spots, closest to the centre, originates in the textured material, whereas the pattern of regular sharp spots at larger distance from the centre is generated by a neighbouring grain.

be expected for stoichiometric BN. No other elements were identified as being present in these agglomerates, except for the small amount of C originating from the TEM sample preparation coating. The edge shape fine structure observed in the EELS spectra of B acquired from these agglomerates and shown in Fig. 7 is almost identical to that of the boron edge taken from a pure BN particle suspended on holey C film and shown in the reference atlas.[7] This indicates that the electron energy levels surrounding the B atom in the textured material observed in our composite sample are the same as those in the pure BN particle. This is another argument for claiming that the boron compound of the textured agglomerates is BN. The formation of BN could also explain why the hardness of ZrO_2 is not substantially increased upon the addition of TiB_2.[6]

Contrast analysis, performed at higher magnifications of the area pointed by arrow B in Fig. 6 indicates an amorphous phase extending between the large titanium boride grain (TiB_{2-x}) and the textured BN microcrystalline agglomerates. The B/N ratio measured in five points of this area are 2.02, 1.14, 1.43, 2.53 and

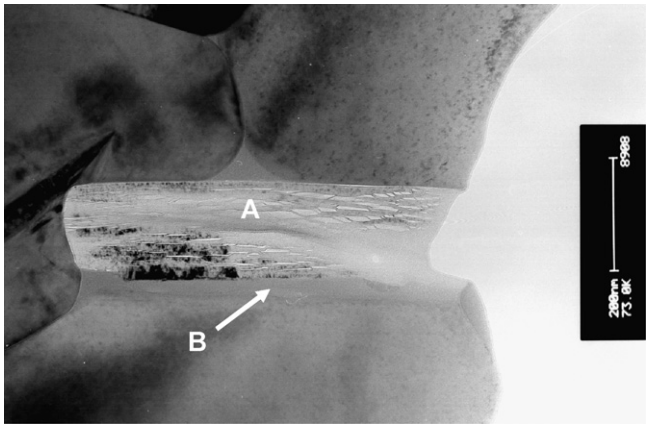

Fig. 6. Higher magnification image of the BN-1 grain shown in Fig. 3. Bar = 200 nm. The image contrast of the area pointed by the arrow B indicates the existence of an amorphous material extending between the large titanium boride grain and the textured agglomeration of BN microcrystallites.

Table 2
Quantitative data obtained by EELS, showing the amounts of boron and nitrogen measured on three grains of microtextured BN agglomerates

Object	Illuminated area[a]	Thickness variation[b] [Fraction of inelastic scattering mean free path]	Measured amount of boron		Measured amount of nitrogen		Calculated B/N ratio	
			No. of B scattering centres (at/nm^2)	Error of no. of B	No. of N scattering centres (at/nm^2)	Error of no. of N	Calculated B/N	Error of calculated B/N
(1)	(2)	(3)	(4)	(5)	(6)	(7)	(8)	(9)
Grain 1	FFB1	ini = 0.5074, fin = 0.6485	4909.73	546.09	5895.11	593.69	0.83	0.12
	FFB1		4858.69	485.86	5895.11	593.69	0.82	0.11
	FFB1		4771.2	530.68	5728.78	576.94	0.83	0.12
	FFB1		4721.61	472.16	5728.78	576.94	0.82	0.11
Grin 2	FFB1	ini = 0.1898, fin = 0.3189	2399.94	267.04	2618.11	291.04	0.91	0.14
	FFB1		2386.85	265.3	2618.11	291.04	0.91	0.14
	FFB1		2356.3	261.81	2618.11	291.04	0.90	0.14
	FFB1		2373.76	237.81	2618.11	291.04	0.90	0.13
	FFB1		2352.08	261.3	2618.11	291.04	0.89	0.14
Grain 3	FFB1	ini = 0.9963, fin = 0.856	4065.68	452.23	4159.35	462.69	0.97	0.15
	FFB1		4197.43	466.88	4283.61	476.52	0.97	0.15

[a] C100 means slightly defocussed beam, illuminating a circular area of approximately 100 nm diameter; FFB1 means fully focussed beam of nominal 1 nm beam diameter; FFB2.2 means fully focussed beam of nominal 2.2 nm beam diameter.
[b] ini means initial thickness, measured by using the first acquired spectrum in the series of spectra for quantification; fin means that we have acquired a last spectrum in the series, for the final thickness evaluation.

1.43. Large amounts of Ti, O and C were detected in this area, besides B and N. The large fluctuations of the measured B/N ratio are indicating a very inhomogeneous composition distribution in the amorphous material. It is only in this kind of narrow strip of amorphous material, formed next to the (TiB_{2-x}) grain in the volume extending from the titanium boride grain to the BN micro-textured agglomerate, that Ti was detected.

Since the hexagonal BN wash-coat applied to the graphite die and punches remains at the interface between the graphite and the sample and, moreover, since BN formation was not observed in ZrO_2–TiN and ZrO_2–TiCN ceramics processed under the same conditions, a reason for the formation of BN has to be found. BN can be formed by reaction of the TiB_2 grains with the nitrogen and oxygen present in the vacuum atmosphere during hot pressing at 1450 °C according to

$$TiB_2 + O_2 + N_2 \Leftrightarrow TiO_2 + 2BN$$

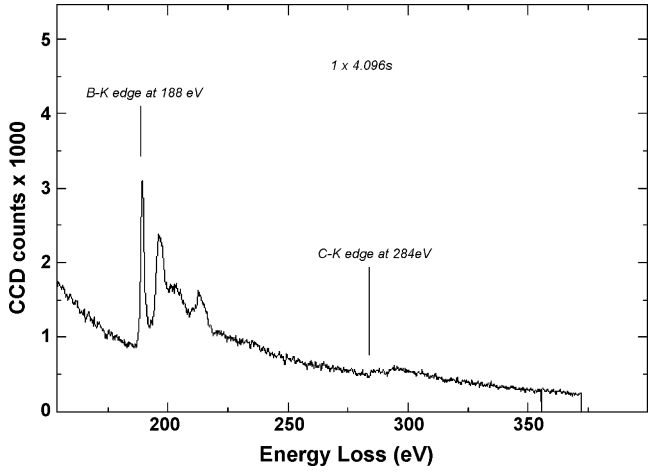

Fig. 7. The boron K-edge fine structure as detected in the textured polycrystalline material (appearing as in Figs. 5 and 6) formed in the composite.

The Gibbs free energy of this reaction, calculated with data taken from,[8] is plotted in Fig. 8, revealing that the formation of BN in the hot pressed ZrO_2–TiB_2 composites is thermodynamically favourable under the applied experimental conditions.

The nitrogen pressure, calculated based on data taken from,[8] in equilibrium with BN is graphically presented as a function of temperature in Fig. 9:

$$2BN \Leftrightarrow N_2 + 2B$$

revealing that BN should be stable in the ZrO_2–TiB_2 composites that were hot pressed below 1600 °C, whereas it should not be stable when hot pressing above 1700 °C.

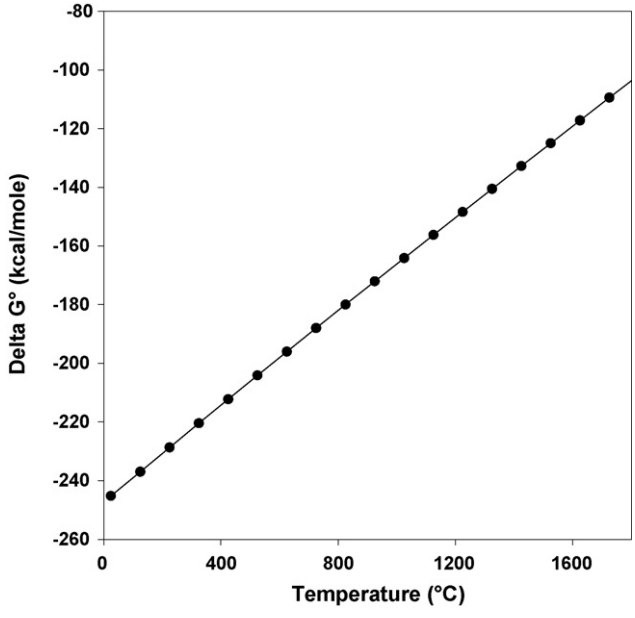

Fig. 8. Standard Gibbs free energy change for the formation of TiO_2 and BN from TiB_2 as a function of temperature.

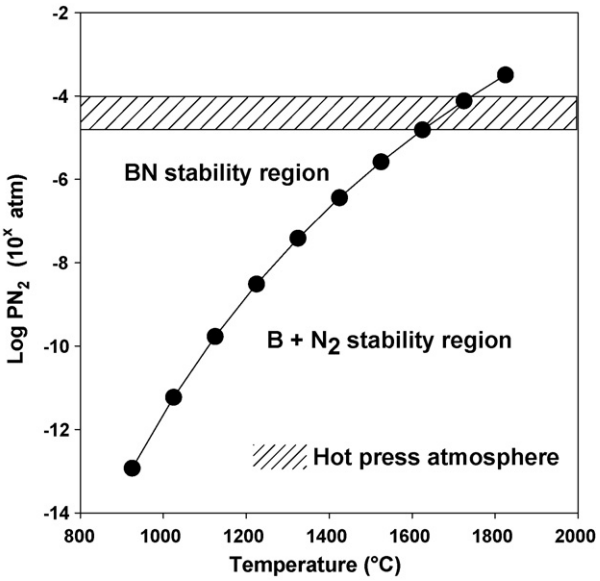

Fig. 9. Furnace atmosphere and calculated nitrogen equilibrium pressure for BN as a function of temperature.

3.3. The zirconia grains

The EELS analysis of the zirconia grains was a much more difficult task because of the significantly smaller grain size, as shown in Fig. 2. Although the ion beam thinning resulted in high angle wedge shapes in the neighbourhood of the main hole, edges of O, Zr and Y were clearly identifiable. No Ti or B edges were observed in the EELS spectra taken inside the zirconia grains.

3.4. The intergranular triple junctions

The spectra acquired on the amorphous material in the triple junctions all revealed significant quantities of B, large quantities of O, Si and Y as well as C (most probably due to sample preparation), but no edges of Ti or Zr. Faint Al edges were observed in the high energy loss range, almost completely embedded in the background. Si is always present as an impurity in the raw powders of zirconia, whereas alumina is an impurity introduced by the mechanical milling media in the powder mixing process, both of these elements allowing the formation of a liquid phase during hot pressing. Large single crystals of alumina were also observed in the sintered composite, as shown in Fig. 1.

4. Conclusions

Massive boron diffusion was observed out of the TiB_2 grains in the ZrO_2–TiB_2 composites hot pressed in vacuum at 1450 °C. The boron forms textured microcrystalline agglomerates of BN mainly surrounding the former TiB_2 grains and dissolves into the intergranular amorphous phase. Single crystal grains with a chemical composition corresponding to non-stoichiometric TiB_{2-x} are left behind. No extended lattice defects are generated inside the titanium boride grains by the diffusion process. Thermodynamic calculations revealed that the formation of BN is favourable under the applied hot pressing conditions.

There is evidence that the excess amount of Ti upon dissolution of B from the TiB_2 grains accumulates both in crystalline inclusions grown inside the TiB_{2-x} grains and in the amorphous material located in-between the large titanium boride grains and the next neighbouring microtextured BN agglomerates.

Titanium was never detected inside the zirconia grains, nor in the Y, Si, O, Al and B containing amorphous intergranular phase filling the triple junctions in-between the zirconia grains. Ti was detected only in the amorphous phase in-between the large titanium boride grains and the BN agglomerate. Zr was never detected in the amorphous intergranular phase, nor inside the titanium boride grains. A stabilisation of the t-ZrO_2 phase by Ti interdiffusion as well as the formation of a (Ti,Zr)B_2 solid solution, as suggested in literature, can therefore be excluded in the ZrO_2–TiB_2 composites hot pressed at 1450 °C. The ZrO_2 phase in the ZrO_2–TiB_2 composites reported here is stabilised exclusively by the overall 2.5 mol% Y_2O_3 incorporated into the system through the ZrO_2 starting powder mixture.

Acknowledgements

Corneliu Sarbu gratefully acknowledges the financial support of the FWO Belgium for a PhD fellowship at the Department of Metallurgy and Materials Engineering of K.U. Leuven.

References

1. Vleugels, J. and Van der Biest, O., Development and characterization of Y_2O_3-stabilized ZrO_2 (Y-TZP) composites with TiB_2, TiN, TiC and $TiC_{0.5}N_{0.5}$. *J. Am. Ceram. Soc.*, 1999, **82**, 2717–2720.
2. Telle, R., Meyer, S., Petzow, G. and Franz, E. D., Sintering behaviour and phase reactions of TiB_2 with ZrO_2 additives. *Mater. Sci. Eng. A*, 1988, **105/106**, 125–129.
3. Watanabe, T. and Shoubu, K., Mechanical properties of hot-pressed TiB_2–ZrO_2 composites. *J. Am. Ceram. Soc.*, 1985, **68**, C-34–C-37.
4. Shoubu, K., Watanabe, T., Drennan, J., Hannink, R. H. J. and Swain, M. V., Toughening mechanisms and microstructures of TiB_2–ZrO_2 composites. In *Advances in Ceramics, Vol. 24-B: Science and Technology of Zirconia III (Proceedings of the Third International Conference on Zirconia'86)*, eds. S. Somiya, N. Yamamoto and H. Yanagida. American Ceramic Society, Westerville, OH, 1988, pp. 1091–1099.
5. Hannink, R. H. J. and Muddle, B. C., Microstructures of zirconia/non-oxide composites. *Mater. Sci. Forum*, 1988, **34–36**, 543–547.
6. Basu, B., Vleugels, J. and Van der Biest, O., Processing and mechanical properties of ZrO_2–TiB_2 composites. *J. Eur. Ceram. Soc.*, 2005, **25**, 3629–3637.
7. EELS Atlas. *A Reference Collection of Electron Energy Loss Spectra Covering All Stable Elements*, eds. C. C. Ahn, O. L. Krivanek, with contributions by R. P. Burgner, M. M. Disko and P. R. Swann. Gatan Inc., Warrendale, PA, USA/HREM Facility, Center for Solid State Science, Arizona State University, Tempe, USA, p. 5.
8. Barin, I. and Knacke, O., *Thermochemical Properties of Inorganic Substances*. Springer-Verlag, Berlin, 1973.